NONLINEAR ROTORDYNAMICS ANALYSIS

Final Report
on
Contract No. NAS8-35992

Prepared for:
George C. Marshall Space Flight Center
Marshall Space Flight Center, AL 35812

Prepared by:
William B. Day
Department of Computer Science and Engineering
Auburn University, AL 36849

15 March 1985

ABSTRACT

This report is an examination of special nonlinearities of the Jeffcott equations in rotordynamics. The immediate application of this analysis is directed toward understanding the excessive vibrations recorded in the LOX pump of the SSME during hot firing ground testing.

Deadband, side force and rubbing are three possible sources of inducing nonlinearity in the Jeffcott equations. The present analysis initially reduces these problems to the same mathematical description. A special frequency, named the nonlinear natural frequency, is defined and used to develop the solutions of the nonlinear Jeffcott equations as singular asymptotic expansions. This nonlinear natural frequency, which is the ratio of the cross-stiffness and the damping, plays a major role in determining response frequencies.

Numerical solutions are included for comparison with the analysis. Also nonlinear frequency-reponse tables are made for a typical range of values.

Finally the regions of stability of these nonlinear problems are bounded using inequalities of the system parameters.

CONTENTS

SECTION		PAGE
1.	Introduction	1
2.	Nondimensionalization and Heuristics	3
3.	General Theory	7
	3.1 Nonlinear Natural Frequency	7
	3.2 Equivalent Problems	8
	3.3 Method of Multiple Scales	9
	3.4 Resonance	10
4.	Examples	12
5.	Stability	14
6.	Conclusions	17
7.	Bibliography	19

LIST OF FIGURES

FIGURE		PAGE
1.	y vs. z - Heuristic example	20
2.	r vs. t - Heuristic example	21
3.	PSD of y - Heuristic example	22
4.	Y vs. Z - Example 1	23
5.	Y vs. Z - Example 1	24
6.	PSD of Y - Example 1	25
7.	PSD of Y - Example 1	26
8.	PSD of Y - Example 1	27
9.	Y vs. Z - Example 2	28
10.	Stability regions	29

LIST OF TABLES

TABLE		PAGE
1.	Frequency response, E=0.5	30
2.	Frequency response, E=1.0	31
3.	Frequency response, E=1.5	32

1. Introduction

Vibrations are inherent in rotating machinery. Mathematical explanations of vibrations began with Jeffcott's description of the shaft's natural frequency of lateral vibration [5]. Unfortunately, Jeffcott's linear model cannot account for all frequencies that have been observed experimentally. In particular, destructive vibrations have occurred in hot firing ground testing of the LOX pump of the SSME with no clue to these vibration's origins being offered by the linear model. Specifically, examination of the power spectral density (PSD) plots reveals unaccountable frequencies. Consequently, numerous investigations have been undertaken to study such rotors and to provide descriptions of the solutions of the two, coupled, second-order differential equations which describe the motion of the rotor's center of mass. Following the early work in rotordynamics by Yomamoto [7], one introduces a nonlinearity to the Jeffcott equations by including the effect of bearing clearance or deadband. In the pump, this deadband refers to the load carriers (ball bearings) and physically describes the clearance between the outer race of the bearing and the support housing. The work of Yomamoto did not include cross-stiffness, but a straight-forward derivation with this modification is easily obtained. A more limiting gap in his work is the assumption that the response is simply a perturbation of the forcing function. This is tantamount to assuming that one always has the graph of a circle as the solution. It is shown in this report that this generally is not the case. Both empirical results by Childs [1,2] and Gupta et al. [4] and numerical solutions using the fourth order Runge-Kutta algorithm by Control Dynamics Company [3] have been helpful in understanding the rotor's motion for the nonlinear problem. This report extends the earlier work by using analytic expressions obtained from singular asymptotic expansions (method of multiple scales) to quantize the solution.

The primary objective of this report is to describe analytically solutions of the nonlinear Jeffcott equations with deadband (or an equivalent variation such as rubbing). To this end emphasis is placed on determining which frequencies one expects from the nonlinear problem, how these frequencies are related to the parameters of the differential equations, and where the solutions are stable.

Section II is a heuristic development of responses to a nonlinear system. This discussion is based on a numerical solution and is intended to help develop some intuition about the solution of the nonlinear problem.

Section III is the formal mathematical development of analytic solutions. This section begins with the discovery of the nonlinear natural frequency and proceeds to incorporate it in an asymptotic expansion of the solution. This leads to considering the two cases of resonant and nonresonant driving

frequencies. Herein also lies an explanation of why one expects the rotor's motion to be either a circle or an annulus.

Section IV contains numerical examples which verify the theoretical expansions. Typical frequency-response descriptions are also included in this part.

Section V discusses bounds for stability regions. This is done with comparison lemmas for majorizing the nonlinear Jeffcott equations.

Section VI concludes the report with a summary of the report's applications and directions for future studies.

2. Nondimensionalization and Heuristics

The linear Jeffcott equations which describe the displacement of the rotor center from its equilibrium position in the inertial, Cartesian coordinate system (y,z) (each in meters) are these:

$$(1.)\quad m\ddot{y}=C_s\dot{y}-K_s y-Q_s z+mu\omega^2\cos\omega t$$

$$(2.)\quad m\ddot{z}=-C_s\dot{z}+Q_s y-K_s z+mu\omega^2\sin\omega t$$

where the shaft of the rotor lies along the x-axis and

m = mass (kg.)

C_s = seal damping (kg./s.)

K_s = seal stiffness (kg./s.^{2})

Q_s = cross-coupling stiffness of seal (kg./s.^{2})

u = displacement of the shaft center of mass from the geometric center (m.)

ω = angular velocity of the shaft (rad./s.)

For the model to include bearing forces which hold the rotor in position, one adds the terms

$$-K_B(y-y\delta/\sqrt{y^2+z^2})+\mu K_B(z-z\delta/\sqrt{y^2+z^2})$$

and

$$-\mu K_B(y-y\delta/\sqrt{y^2+z^2})-K_B(z-z\delta/\sqrt{y^2+z^2}),$$

respectively, to right-hand sides of equations (1.) and (2.)

Here

K_B = bearing stiffness (kg./s.^{2})

δ = clearance or deadband between housing and bearing (m.)

μ = coefficient of friction between housing and bearing (none).

These bearing forces occur only when $\sqrt{y^2+z^2}>\delta$; otherwise, they are zero. Since μ is nondimensional and typically small, one may regard it as zero without affecting the qualitative results.

Equations (1.) - (2.) then become

$$(3.)\quad \ddot{y}+(C_s/m)\dot{y}+(1/m)[K_s+K_B(1-\delta/r)]y+(Q_s/m)z=u\omega^2\cos\omega t$$

$$(4.)\quad \ddot{z}+(C_s/m)\dot{z}-(Q_s/m)y+(1/m)[K_s+K_B(1-\delta/r)]z=u\omega^2\sin\omega t$$

when $r=\sqrt{y^2+z^2}>\delta$; otherwise, $K_B=0$. Equations (3.) - (4.) can be put in nondimensional form using a displacement g and a frequency σ. One pair of candidates for g and σ would be $g=\delta$, the deadband size, and $\sigma^2=\omega_0^2=K_s+K_B$, the natural frequency of the

corresponding linear problem ($\delta=0$). Thus, using $Y=y/g$, $Z=z/g$, and $\tau=\sigma t$, the dimensionless equations are these:

(5.) $Y''+CY'+[A+k(1-\Delta/R]Y+BZ=E\phi^2\cos\phi\tau$

(6.) $Z''+CZ'-BY+[A+k(1-\Delta/R)]Z=E\phi^2\sin\phi\tau$

where prime denotes differentiation with respect to τ and $C=C_S/m/\sigma$, $A=K_S/m/\sigma^2$, $k=K_B/m/\sigma^2$, $B=Q_S/m/\sigma^2$, $\Delta=\delta/g$, $R=r/g$, $E=u/g$, and $\phi=\omega/\sigma$.

Equations (5.) - (6.) can be reduced to the following single equation by defining $W=Y+iZ$:

(7.) $W''+CW'+\{A+k(1-\Delta/|W|)-iB\}W=E\phi^2\exp(i\phi\tau)$

Furthermore, the polar form of equations (5.) - (6.) is

(8.) $R''+CR'+[A+k(1-\Delta/R)-(\Theta')^2]R=E\phi^2\cos(\phi\tau-\Theta)$

(9.) $R\Theta''+(2R'+CR)\Theta'=R[B-\mu k(1\Delta/R)]+E\phi^2\sin(\phi\tau-\Theta)$

where $R=(Y^2+Z^2)^{1/2}$ and $\Theta=\text{Arctan}\ (Z/Y)$.

The nondimensional Jeffcott equations with deadband and mass imbalance are easily solved numerically using a fourth-order Runge-Kutta algorithm. If these solutions are then plotted and analyzed in a power spectral density (PSD) investigation, the resulting graphs provide a direction for initial, analytic descriptions. To this end, consider the following special case:

$m=1.$	$u=1.5\delta$
$C=240.$	$Q=200,000.$
$K_S=0.$	$\delta=.0000285$
$K_B=1,305,000.$	$\omega=500\text{Hz}$

The units used are those given after equations (1.) - (2.) and are only of interest in a relative sense. Therefore, with $\omega_0=(1,305,000)^{1/2}$ and $\delta=.0000285$ as the nondimensionalizing parameters, the Jeffcott equations become

$$Y''+(C_S/\omega_0)\,Y'+(1-1/R)Y+(Q_S/\omega_0^2)\;Z=1.5(\omega/\omega_0)^2\cos(\omega/\omega_0)\tau$$

$$Z''=(C_S/\omega_0)\,Z'-(Q_S/\omega_0^2)\;Y+(1-1/R)\;Z=1.5(\omega/\omega_0)^2\sin(\omega/\omega_0)\tau$$

where $\tau=\omega_0 t$ and $R=(Y^2+Z^2)^{1/2}=(y^2+z^2)^{1/2}/\delta$. Figure 1 shows the motion for this case. The motion has become periodic for the time interval ($.5<=t<=1.$s.) shown. The graph of t vs. $r=\delta R$, given in Figure 2, suggests that r has the form

$$r=.71+.39\cos720\pi\ t=a_0+a_1\cos\gamma\tau.$$

It is this form that leads one to consider approximating the Jeffcott equations with

$$Y''+CY'+(1-1/(a_0+a_1\cos\gamma\tau))Y+BZ=1.5\phi^2\cos\phi\tau$$

$$Z''+CZ'-BY+(1-1/(a_0+a_1\cos\gamma\tau))Z=1.5\phi^2\sin\phi\tau.$$

Examination of the PSD of R shows that R is actually an infinite sum:

$$R=\sum_{k=0}^{\infty} a_k\cos k\gamma\tau$$

with a_0 and a_1 the dominant terms. The other coefficients decrease exponentially to zero as $k\to\infty$. Therefore, the replacement of R with $a_0+a_1\cos\gamma\tau$ is a reasonable approximation. Furthermore, a_0 can be considered the average value of R. Since this value will be nonnegative, one may write:

$$1/R=1/(a_0+a_1\cos\gamma\tau)$$

$$=(1/a_0)\sum_{k=0}^{\infty}(-a_1/a_0)^k(\cos\gamma\tau)^k.$$

If the original infinite summation of R had been used, the above series for 1/R would still be a summation of $\cos\gamma\tau$ terms, but with different coefficients.

Now consider a_1/a_0 as an asymptotic expansion parameter ε. Thus:

$$1/R=(1/a_0)[1-\varepsilon\cos\gamma\tau]+O(\varepsilon^2).$$

This last approximation may ultimately lead to poor approximations for the magnitudes (but not the frequencies) of the Jeffcott solutions since higher (k>1) powers of $\cos\gamma\tau$ actually contribute to the coefficient of $\cos 0\tau$ and $\cos\gamma\tau$. Therefore, the following derivation for a straightforward asymptotic expansion may be used primarily for predicting response frequencies, but will generally be poor for describing the corresponding magnitudes.

With this prelude, one replaces the nonlinearity 1/R of the Jeffcott equations with $1/a_0-\varepsilon\cos\gamma\tau$ and expands the solution as $Y=Y_0+\varepsilon Y_1+O(\varepsilon^2)$ and $Z=Z_0+\varepsilon Z_1+O(\varepsilon^2)$. The resulting low-order problems are these:

O(1):

$$Y_0''+CY_0'+(1-1/a_0)Y_0+BZ_0=1.5\phi^2\cos\phi\tau$$

$$Z_0''+CZ_0'-BY_0+(1-1/a_0)Z_0=1.5\phi^2\sin\phi\tau$$

O(ε):

$$Y_1''+CY_1'+(1-1/a_0)Y_1+BZ_1=-(1/a_0)(\cos\gamma\tau)Y_0$$

$$Z_1''+CZ_1'-BY_1+(1-1/a_0)Z_1=-(1/a_0)(\sin\gamma\tau)Z_0$$

The prescribed initial conditions are used with the zero-order problem. The initial conditions for all higher-order problems are all zero.

There is a circular argument involved here. One is using the answer, which was found numerically, to solve the problem. Although this is unacceptable mathematics, the results obtained in this heuristic discussion are not derived solutions but only suggestions of solutions. With this in mind, one proceeds to solve the zero - and first-order problems. The zero-order problem has solutions of the form:

$$Y_0 = C_1(\tau)\sin\beta\tau + C_2(\tau)\cos\beta\tau + C_5\cos\phi\tau - C_6\sin\phi\tau$$

$$Z_0 = C_3(\tau)\sin\beta\tau + C_4(\tau)\cos\beta\tau + C_5\sin\phi\tau + C_6\cos\phi\tau$$

where C_1, C_2, C_3 and C_4 are all functions of time and all involve decaying exponential functions. Thus, in steady-state

$$Y_{0,ss} = C_7\cos(\phi\tau + \phi_0)$$

$$Z_{0,ss} = C_7\sin(\phi\tau + \phi_0)$$

In the first-order problem, one is presented with the same left-hand side as the zero-order problem. Thus, in steady-state it is only the forcing function of the right-hand side that provides non-trivial solutions. Hence, one finds combinations of the form $\cos\gamma\tau\cos\phi\tau$ and $\sin\gamma\tau\sin\phi\tau$.

Thus, the steady-state solutions of the first-order problem should look like these:

$$Y_1 = C_8\cos(\phi \pm \gamma)\tau$$

$$Z_1 = C_8\sin(\phi \pm \gamma)\tau$$

Since higher order problems contain right-hand sides of the form

$$(\cos k\gamma t)\, f(Y_0, Z_0, Y_1, Z_1, \ldots, Y_{k-1}, Z_{k-1}),$$

it follows by induction on k that the kth-order steady-state solutions contain terms of the form

$$Y_k \sim \cos(\phi \pm k\gamma)\tau$$

$$Z_k \sim \sin(\phi \pm k\gamma)\tau$$

Finally, one anticipates that the PSD of Y (or equivalently Z) will show frequencies at $\phi \pm k\gamma$. This is verified in Figure 3, which is the PSD of the (numerical) solution of the test problem.

3. General Theory

3.1 Nonlinear Natural Frequency

Consider the homogeneous (E=0) equation corresponding to equation (7.). If this equation were also linear ($\Delta=0$), then exponentially growing or decaying solutions would generally result for a given set of system parameters. In the special case that $(B/C)^2=A+k$, a sinusoidal solution is obtained with frequency $\beta=B/C$. To see this, consider the characteristic equation for $W=\exp(m\tau)$:

$$m^2+Cm+[A+k-iB]=0$$

$$m=-C/2\pm\{C^2/4-A-k+iB\}^{1/2}=-C/2\pm\{C^2/4-(B/C)^2+iB\}^{1/2}$$

$$m=-C/2\pm i\{iC/2-B/C\}^{1/2}=-C-iB/C,\ iB/C.$$

In the nonlinear, homogeneous problem, k is replaced by $k(1-\Delta/R)$; hence, if R is a constant, then there is a wide spectrum of R for which $(B/C)^2$ may be $A+k(1-\Delta/R)$; i.e., if

$$(10.)\quad A<(B/C)^2\leq A+k,$$

then there is a constant value of R (with $R>\Delta$) for which $(B/C)^2=A+k(1-\Delta/R)$. This value of R is denoted by a and the corresponding frequency by $\beta_0=B/C$. This frequency is labeled the nonlinear natural frequency. Thus, whenever inequality (10.) is satisfied, equations (5.) - (6.) with E=0 have steady-state solutions $Y=a\cos(\beta_0\tau)$ and $Z=a\sin(\beta_0\tau)$.

The same results can be found from the polar equations (8.) - (9.) by assuming R and Θ' are constants. Then with E=0 those equations become

$$[A+k(1-\Delta/R)-(\Theta')^2]R=0,\quad C\Theta'=B.$$

Thus, $\beta_0=\Theta'=B/C$ and $a=R=k\Delta/(A+k-\beta_0^2)$.

Notice that $\beta_0=B/C\leq(A+k)^{1/2}=\omega_0$, the dimensionless natural frequency of the linear system. Thus, in considering the general nonhomogeneous problem, it is necessary to be aware of these three dimensionless frequencies:

β_0 - the nonlinear natural frequency,

ω_0 - the natural frequency,

ϕ - the driving frequency.

Either β_0 or ω_0 is an appropriate choice for σ, the nondimensionalizing frequency. Correspondingly, one would select either a (with β_0) or u (with ω_0) as the base displacement g.

One final rearrangement of equation (7.) is made here to emphasis the nonlinear natural frequency:

(11.) $W''+CW'+\kappa W=f(W)+E\phi^2\exp(i\phi\tau)$

where $\kappa=A+k(1-\Delta/a)-iB$ and $f(W)=k\Delta[1/|W|-1/a]W$.

3.2 Equivalent Problems.

In this subsection the forcing function is assumed to have the form $F(\omega)\exp(i\omega t)$, where $F(\omega)>=0$ (or equivalently $F(\omega)$ [illegible]) and F is single-valued for $\omega>=0$. The following are special cases of physical interest:

a. Mass imbalance. As discussed above, $F(\omega)=u\omega^2$ for a mass u.

b. Side Force. This force may be introduced into the Jeffcott equations (1.) - (2.) as constant replacements for the mass imbalance. In such cases, equation (7.) becomes:

$$W''+CW'+\{A+k(1-\Delta/|W|)-iB\}W=u\omega^2/\delta g^2=\text{constant}.$$

Thus, a side force is the special case $F(\omega)$=constant and $\omega=0$.

c. Rubbing. Rubbing contact between a rotor and its housing produces a Coulomb damping force. This force would modify the original Jeffcott equations by the addition of the terms:

$$K_{st}(1-\delta/r)y-\mu K_{st}(1-\delta/r)z+K_{st}(1-\delta/r)G$$

and $$\mu K_{st}(1-\delta/r)y+K_{st}(1-\delta/r)z+\mu K_{st}(1-\delta/r)G$$

respectively, to the right-hand sides of equations (1.) - (2.). Here, G=constant=stator offset in the y-direction, K_{st}=stator stiffness and μ=coefficient of friction, which may not be small. As before these forces would be included only when $r=(y^2+z^2)^{1/2}>\delta$. On replacing y-G by y, equation (7.) (and correspondingly its equivalent forms) again occurs but with these modifications:

1. $i[-B]$ is replaced by $i[-B+\mu(K_{st}/g^2)(1-\Delta/R)]$

2. the forcing function $E\phi^2\exp(i\phi\tau)$ is replaced by $E\phi^2\exp(i\phi\tau)+(-\omega_0^2/g^2)(G/\delta)$.

If the mass imbalance term is omitted, then one may regard the deadband with side force problem and the rubbing problem as equivalent. Notice that the range of values of the parameters for these two problem may not be the same since the rubbing problem includes the non-negligible term $\mu(K_{st}/g^2)(1-\Delta/r)$.

3.3 Method of Multiple Scales.

Now consider a more formal development of analytic solutions. Straight-forward asymptotic expansions are not general enough for this problem since they always lead to a zero-order approximation of the form:

$$W = M \exp(i\beta_0 \tau) + N \exp(i\phi\tau).$$

The heuristic example considered in section 2 suggests that $\beta_0\tau$ must be replaced by $\beta(\tau)$ which is close to but not exactly $\beta_0\tau$. There are several methods of attacking such singular problems; these are described in Nayfeh [6]. One method, the method of averaging, is appropriate for the Jeffcott equations since it begins with the assupmtion that $W = M(\tau) \exp(i\beta(\tau)) + N \exp(i\phi\tau)$. Another method, multiple scales, is also appropriate because one can envision the action of the rotor being based on two different time scales. The following development uses the method of multiple scales. The results are identical for the method of averaging. In this subsection the forcing frequency ϕ is restricted to differ from the nonlinear frequency β ; i.e., the problem is not resonant. Resonance, $\beta = \phi$, is dealt with in the following subsection.

Instead of one time scale τ, assume the problem depends on many time scales:

$$T_0 = \tau, \quad T_1 = \varepsilon\tau, \quad T_2 = \varepsilon^2\tau, \quad \ldots$$

Henceforth, only T_0 and T_1 are used. Let $W(\tau) = W(T_0, T_1) = W_0(T_0, T_1) + \varepsilon W_1(T_0, T_1) + \ldots$ Equation (11.) becomes a partial differential equation since

$$d/d\tau = (\partial/\partial T_0)(dT_0/d\tau) + (\partial/\partial T_1)(dT_1/d\tau) = D_0 + \varepsilon D_1$$

and $(d^2/d\tau^2) = (D_0 + \varepsilon D_1)^2$.

Thus, one finds

$$(12.)\quad (D_0 + \varepsilon D_1)^2 (W_0 + \varepsilon W_1 + \ldots) + C(D_0 + \varepsilon D_1)(W_0 + \varepsilon W_1 + \ldots) + \kappa (W_0 + \varepsilon W_1 + \ldots) = \varepsilon f(W_0 + \varepsilon W_1 + \ldots) + E\phi^2 \exp(i\phi T_0).$$

Equating like powers of ε yields

$$(13.)\quad \varepsilon^0 : D_0^2 W_0 + C D_0 W_0 + \kappa W_0 = E\phi^2 \exp(i\phi T_0).$$

This is a linear problem with this steady-state solution

$$W_0 = M \exp(i\beta_0 T_0) + N \exp(i\phi T_0)$$

where $N = E\phi^2/(-\phi^2 + iC\phi + \kappa)$ and $M = M(T_1)$. To determine M one must examine the ε-order problem and choose M to eliminate secular terms; see Nayfeh [6]:

$$\epsilon^1: D_0^2 W_1 + C W_1 + \kappa W_1 = -2 D_0 D_1 W_0 - C D_1 W_0 + f(W_0).$$

With $L = k\Delta/\epsilon$, the right-hand side of the last equation becomes

$$-2i\beta_0 M' \exp(i\beta_0 T_0) - C M' \exp(i\beta_0 T_0)$$

$$+ L(1/|W_0| - 1)\,[M \exp(i\beta_0 T_0) + N \exp(i\phi T_0)]$$

where $|W_0| = \{|M|^2 + |N|^2 + \bar{M}N \exp[i(\phi - \beta_0)T_0] + M\bar{N} \exp[i(\beta_0 - \phi)T_0]\}^{1/2}$

To avoid secular terms one requires that the collective coefficient of $\exp(i\beta_0 T_0)$ be zero. Although an analytic solution of the differential equation for $M(T_1)$ has not been found, one can qualitatively assess M based on a similar problem (van der Pol's equation) and specific numerical results (presented in the next section).

Since $M(T_1)$ is complex, it may be written as $M(T_1) = \rho(T_1)\exp[i\hat{\beta}(T_1)]$. Thus,

$W_0 = \rho(T_1)\exp[i\beta_0 T_0 + i\hat{\beta}(T_1)] + N \exp(i\phi T_0)$ or, assuming $\hat{\beta}(T_1)$ is analytic near $t=0$, $W_0 = \rho(T_1)\exp[i(\beta_0 + \epsilon\beta_1)\tau + \ldots] + N \exp(i\phi\tau)$. Thus the fundamental frequency of the nonlinear problem is not β_0 but $\beta = \beta_0 + \epsilon\beta_1 + \ldots$; however, β must reduce to β_0 when $E\phi^2 = 0$. This frequency shift can account for the phenomenon of "tracking" that has been observed experimentally [2]. Similarly, the frequency $\gamma = \phi - \beta_0$ that appears in the expression for $|W_0|$ should be considered as $\gamma = \phi - \beta$. Then $1/|W_0|$ shows all frequencies $n\gamma$ and $W_0/|W_0|$ shows all frequencies $n\gamma \pm \beta$, for $n = 0, 1, \ldots$ This suggests that M has a complex Fourier series of the form:

$$\sum_{n=-\infty}^{\infty} s_n \exp(in\gamma T_1).$$

Another factor of M must also be included since numerical examples show that $M \equiv 0$ if $E\phi^2$ is greater than some fixed value. This is similar to the behavior of the van der Pol oscillator; see [6]. Thus, one may speculate that M has a factor of the form $F = 1/[1 + \exp(-\eta T_1)]$ where $\eta = \eta(E\phi^2)$. This would imply that $F \to 1$ as $\tau \to \infty$ when $\eta \geq 0$ and $F \to 0$ as $\tau \to \infty$ when $\eta \leq 0$. Thus, M looks like:

$$1/[1 + \exp(-\eta T_1)] \sum_{n=-\infty}^{\infty} s_n \exp(in\gamma T_1).$$

PSD plots of R show only frequencies of $n\gamma$ while plots of Y show frequencies of ϕ and $n\gamma \pm \beta$.

3.4 Resonance.

The resonance problem $\beta = \omega$ can be handled in a manner quite similar to the nonresonance case. The approximation $\phi = 1 + \sigma E$ is made where E is the nondimensional mass causing the imbalance and β_0 is the nondimensionalizing frequency. With the same multiple scale expansion as before, one finds the following two low-order problem:

$O(1)$: $\partial^2 W_0/\partial T_0^2+C(\partial W_0/\partial T_0)+[1-1/a-iB]W_0=0$

with the solution $W_0=m(T_1)\exp(iT_0)$,

$O(E)$: $\partial^2 W_1/\partial T_0^2+C(\partial W_1/\partial T_0)+[1-1/a-iB]W_1+2\partial^2 W_0/\partial T_0\partial T_1+$

$C(\partial W_0/\partial T_1)=(1/E)(1/|W_0|-1/a)W_0+\exp(iT_0)\exp(i\sigma T_1)$.

Elimination of the secular terms of the latter equation requires

$$0=-2i M'\exp(iT_0)-CM'\exp(iT_0)+(1/E)(1/M-1/a)M\exp(iT_0)+\exp(i\sigma T_1)\exp(iT_0)$$

or with $M = m(T_1)\exp(i\alpha(T_1))$

$$(2i+C)(m'+i\alpha' m)=(m/E)(1/m-1/a)+\exp(i\sigma T_1)\exp(-i\alpha).$$

Now let $\psi=\sigma T_1-\alpha$, separate real and imaginary parts, square both sides of the two resulting equations and add to find the steady-state solution ($m'=0=\alpha'$):

$$m^2(1/a^2-4\sigma/a+\sigma^2(c^2+4))+m(-2/a+4\sigma)=0.$$

This magnitude result, a quadratic equation, is identical to that of Yomamoto [7] although the expansion there is with the base $\exp(i\phi T_0)$.

$$W=m\exp(i(T_0+\alpha))$$

where m is found above and the frequency is

$$(d/dt)(T_0+\alpha)=(d/dt)(t+\sigma Et-\psi).$$

But $d\psi/dt=0$. Thus, the frequency is $1+\sigma E=\phi$. This phenomenon is often referred to as entrainment; i.e., the nonlinear frequency, β, is entrained by the forcing frequency, ω.

4. Examples.

This section contains three numerical examples of the theory presented in Section 3. The first example shows how the solution changes for a fixed forcing frequency but increasing forcing magnitudes. Example 2 is similar to the first example but with a different set of parameters. Example 3 is a frequency-response illustration of variations in the forcing frequency and corresponding responses.

Example 1. In this example the system constants used are these: $\mu=0$, $m=1$ lb.-s.^{2}/in., $C_s=240$ lb.-s./in., $K_s=0.$, $K_b=1{,}305{,}000$ lb./in., $Q_s=200{,}000$ lb./in., $\delta=.0000285$ in., and $\omega^b=500$ Hertz$=1000\pi$ rad./s. Thus, $\beta_0=833.33$ rad./s. and $a=.000060915$ in. The system is made nondimensional using a for the g-displacement and β for the σ-frequency. With these choices, the constants of this equation:

$$W''+CW'+[k(1-\Delta/|W|)-iB]W=E\phi^2\exp(i\phi\tau)$$

have these values: $C=.288$, $k=1.8792$, $\Delta=.467865$, $B=.288$, and $\phi=6\pi/5$.

Figures 4 and 5 show changes in the solution Y vs. Z as E assumes the values $100n/(1000\pi)^2$ a for $n=0,1,\ldots,7$. The graphs are plotted for $.2<t\leq.5$s. The initial circle (for $E=0$) opens into an annular region, which becomes larger and thicker as E increases until a (transition) value of E occurs and the coefficient of $\exp(i\beta\tau)$ becomes zero. Thus, $W=N\exp(i\phi\tau)$, a circle of radius $|N|$. As E increased beyond this transition value, the solution remains a circle (figure 2.d) with radius $|N|=|E\phi^2/(-\phi^2+iC\phi+k(1-\Delta/|N|)-iB)|$.

The nonlinear natural frequency β_0 is the angular frequency of the circle when $E=0$, but this frequency increases as E increases. This tracking phenomenon is displayed in the PSD plots of figures 6 and 7 using the dimensional frequency β. In these figures only the 120-180 Hertz range is shown. At $E=7/10{,}000\pi^2 a$, there is no frequency in this range; instead, the circle is tranversed at the forcing frequency, ω.

Figure 8, a typical full PSD plot, is the case $E=4/10{,}000\pi^2$ a. As shown earlier, one expects frequencies of ω and β to appear, as well as harmonics of $n\gamma\pm\beta$ where $\gamma=\omega-\beta$ and $n=1, 2,\ldots$ Thus, with $\beta=150$ Hertz, and $\omega=500$ Hertz, one predicts that the PSD plot will exhibit peaks at 150, 200, 500, 550, 850, 900,...Hertz. Figure 8 confirms these predictions.

Example 2. In this example, the system constants from CDC[3] are these: $\mu=0$, $m=.20422$ lb.-s.^{2}/in., $C=200$ lb.-s./in., $K_s=200{,}000$ lb./in., $K_b=1{,}000{,}000$ lb./in., $\omega=500$ Hertz, $Q_s=C_s\omega/2$ lb./in., and $\delta^b=.0005$ in. Thus, $\beta=250$ Hertz $=500\pi^s$ rad./s. and $a=.0007183$ in. Figure 9 summarizes changes in Y vs. Z as E varies by $250n/(1000\pi)^2$ a, $n=0, 1,\ldots,4$. These

graphs are plotted for $.45<t\leq.5s$.

In general, if the time interval is sufficiently large, the plots of annular regions will be completely filled (visually if not mathematically). However, when the ratio of β to γ is p/q for small, positive integers p and q, then the curve actually falls on itself as time evolves and some attractive patterns appear. Figure 9.d is a case where $\beta/\gamma=5/4$, and the picture would look essentially the same whether shown for $.45<t\leq.5s$. (actual) or for $.45<t\leq50s$. On the other hand, figure 6.c is more typical and would show a black annulus for $.45<t\leq50s$.

Example 3.

As described above, one expects either a circle or an annulus at each fixed forcing frequency ϕ. Furthermore, near resonance one always finds a circle since the characteristic frequency is entrained by the forcing frequency. Considering that the forcing function is a continuous function of this frequency ϕ, it follows that the solution is a circle or an annulus over an interval of the ϕ-axis and that the number of transitions between the two shapes is finite over a bounded portion of the positive ϕ-axis.

TABLES I, II, and III illustrate these results for the problem with these parameter values:

$C_s=240./\omega_0$ $\qquad$ $\delta=.0000285$

$Q_s=200{,}000./\omega_0^2$ $\qquad$ $F=0.5$, 1.0, or 1.5

$K_s=0.$ $\qquad$ $K_s=1{,}305{,}000.=\omega_0^2$

Tables I, II, and III are for the three cases E=0.5, 1.0, 1.5, respectively. In all three cases, ω_0 is used as the nondimensionalizing frequency. Each of the three tables describes the response curve by listing the radius of circles or the inner and outer radii for annuli. Furthermore, the frequency $\gamma=|\beta-\omega|$ is given for annuli. The values listed for ϕ are every 0.1 except when

1. more refinement is required to bound better the transition point
2. less refinement is needed because of small variation in the response at different frequencies.

Particular attention should be paid to Table III since this table shows three different regions in which the circle appears as the solution. The first two tables contain only one such region.

5. Stability.

To examine questions of stability for the nonlinear Jeffcott equations, it is helpful to use the following complex form:

$$\ddot{w}+C_s\dot{w}+[K_B+K_s(1-\delta/r)-iQ_s]w=F(u,\omega)$$

where $w=y+iz$. Since the solution's stability is determined by the corresponding homogeneous equation, one has

$$\ddot{w}+C_s\dot{w}+[K_B+K_s(1-\delta/r)-iQ_s]w=0.$$

Furthermore, if a solution becomes unbounded then $r > r_0$ for all constants r_0. Thus, as a comparison one may consider

$$\ddot{w}+C_s\dot{w}+[K_B+K_s(1-\delta/r_0)-iQ_s]w=0.$$

Solutions of this equation are of the form $w=\exp(Mt)$. Hence:

$$m^2+C_s m+[K_B+K_s(1-\delta/r_0)-iQ_s]=0.$$

The stability question is reduced to determining whether $Re(m)<0$. But

$$m=-C_s/2 \pm [(C_s/2)^2-K_B-K_s(1-\delta/r_0)+iQ_s]^{1/2}$$

and

$$Re(m)=-C_s/2 \pm Re[C_s^2/4-K_B-K_s(1-\delta/r_0)+iQ_s]^{1/2}$$
$$=-C_s/2 \pm Re[C_1+iC_2]^{1/2}$$

where

$$C_1=C_s^2/4-K_B-K_s(1-\delta/r_0)$$
$$C_2=Q_s.$$

In this modified form, the stability question becomes this:

Solutions are stable if and only if $Re(C_1+iC_2)^{1/2}<C_s/2$.

The following lemmas are useful for bounding the value of Q_s/C_s in order to find stable solutions.

Lemma 1. $Re(C_1+iC_2)^{1/2}=(|C_1|/2)^{1/2}[(1+(C_2/C_1)^2)^{1/2}\pm 1]^{1/2}$ where the minus sign is used for $C_1<0$.

Proof: Case $C_1<0$. $C_1<0$ implies $|C_1|=-C_1$. Then:

$$Re(C_1+iC_2)^{1/2}$$
$$=(C_1^2+C_2^2)^{1/4}\cos[1/2\ \ \mathrm{Atan}(C_2/-|C_1|)]$$

$$=(C_1^2+C_2^2)^{1/4}\cos[(\pi-\theta)/2]$$

where $\theta = \text{Atan}(C_2/|C_1|)$

$$=(C_1^2+C_2^2)^{1/4}\sin(\theta/2)$$

$$=(C_1^2+C_2^2)^{1/4}[(1-\cos\theta)/2]^{1/2}$$

$$=(C_1^2+C_2^2)^{1/4}(1/2)^{1/2}[1-|C_1|/(C_1^2+C_2^2)^{1/2}]^{1/2}$$

$$=1/2^{1/2}[(C_1^2+C_2^2)^{1/2}-|C_1|]^{1/2}$$

$$=(|C_1|/2)^{1/2}[(1+(C_2/C_1)^2)^{1/2}-1]^{1/2}$$

Case $c_1>0$. $C_1>0$ implies $C_1=|C_1|$. Then

$$\text{Re}(C_1+iC_2)^{1/2}$$

$$=(C_1^2+C_2^2)^{1/4}\cos[1/2\ \text{Atan}(C_2/|C_1|)]$$

$$=(C_1^2+C_2^2)^{1/4}[(1+\cos\ \text{Atan}\ C_2/|C_1|)/2]^{1/2}$$

$$=(C_1^2+C_2^2)^{1/4}[(1+|C_1|/(C_1^2+C_2^2)^{1/2})/2]^{1/2}$$

$$=1/2^{1/2}[(C_1^2+C_2^2)^{1/2}+|C_1|]^{1/2}$$

$$=(|C_1|/2)^{1/2}[(1+(C_2/C_1)^2)+1]^{1/2}.$$

Lemma 2. If $(Q_s/C_s)^2<K_B$, then for all $\delta \le r_0 < \infty$,

$$\text{Re}(C_1+iC_2)^{1/2}<C_s/2.$$

Proof: Case $C_1<0$. If $C_1<0$, then $|C_1|=-C_1$.

$$(Q_s/C_s)^2<K_B$$

$$-K_B<-(Q_s/C_s)^2$$

$$-(K_s+K_B(1-\delta/r_0)) < -K_B < -(Q_s/C_s)^2$$

$$C_1=(C_s/2)^2-(K_s+K_B(1-\delta/r_0)) < (C_s/2)^2-(Q_s/C_s)^2$$

$$-|C_1| < (C_s^4-4Q_s^2)/4C_s^2$$

$$-4C_s^2\,|C_1| < C_s^4-4Q_s^2$$

$$4Q_s^2 < C_s^4+4C_s^2\,|C_1|$$

$$4(Q_s^2+C_1^2) < C_s^4+4C_s^2\,|C_1|+4|C_1|^2$$

$$4(Q_s^2+C_1^2) < (C_s^2+2|C_1|)^2$$

$$2|C_1|[1+(Q_s/C_1)^2]^{1/2} < C_s^2+2|C_1|$$

$$[1+(Q_s/C_1)^2]^{1/2} < C_s^2/2|C_1|+1$$

$$|C_1|/2([1+(Q_s/C_1)^2]^{1/2}-1) < C_s^2/4$$

$$(|C_1|/2)^{1/2}([1+(Q_s/C_1)^2]^{1/2}-1) < C_s/2.$$

But by Lemma 1, the last left-hand side is $\mathrm{Re}(C_1+iC_2)^{1/2}$. Thus,

$$\mathrm{Re}(C_1+iC_2)^{1/2} < C_s/2.$$

Case $C_1 > 0$. This case is identical to the previous argument except that one has $+|C_1|$ instead of $-|C_1|$ on the fifth line of the inequalities and thereafter the corresponding term switches signs.

Lemma 3. If $(Q_s/C_s)^2 > K_B+K_s$, then for all $\delta \leq r_0 < \infty$,

$$\mathrm{Re}(C_1+iC_2)^{1/2} > C_s/2.$$

Proof: After noting

$$(Q_s/C_s)^2 > K_B+K_s > K_B+K_s(1-\delta/r_0)$$

one has

$$-K_B-K_s(1-\delta/r_0) > -(Q_s/C_s)^2$$

and

$$C_1=-K_B-K_s(1-\delta/r_0)+(C_2/2)^2 > (C_s/2)^2-(Q_s/C_s)^2$$

The remaining steps in the derivation are identical to Lemma 2 for both cases of C_1 except that the inequalities are reversed. Thus, $\mathrm{Re}(C_1+iC_2)^{1/2} > C_s/2$.

Figure 10 summarizes the stable and unstable regions as functions of $(Q_s/C_s)^2$ for the linear and nonlinear homogeneous problems. In this figure, there is only one point on the $(Q_s/C_s)^2$-axis at which oscillations may occur for the linear problem. For the nonlinear case, oscillation and hence transition between stable and unstable still occurs at only one point on the $(Q_s/C_s)^2$-axis, but that point may be anywhere between K_B and K_B+K_s.

6. Conclusions

This report has shown how vibrations at frequencies which are unexplainable by linear theory can be expected in nonlinear Jeffcott models which consider deadband, side forces or rubbing. These frequencies and their regions of stability are bounded by parameters of the differential equations. Although the asymptotic analysis is weak in quantizing exactly the frequencies and the corresponding magnitudes, there exists simple numerical methods which may be employed for the desired precision. The analysis, then, serves as a guide in locating nonlinear vibrations, which the numerical techniques then find accurately. This will apply to systems of higher degrees of freedom as well.

In studying the Jeffcott rotor with deadband or rubbing and sinusoidal forcing (including constant side force), one must consider these three frequencies: (a) the forcing frequency ω; (b) the natural frequency, ω_0, of the associated linear problem (deadband= δ =0); and (c) the nonlinear natural frequency β_0. The frequency ω depends only on the forcing function; ω_0 depends only on the system parameters; β, with its base value β_0, depends on both the forcing function and the system parameters. For a specific set of equation parameters, one can find this nonlinear natural frequency β_0 as the ratio of cross-stiffness to damping and then use it with the (linear) natural frequency to bound the frequencies β.

For a given system and a nonzero, external, sinusoidal force, the y-z response is either a circle at the forcing frequency or an annulus composed of the (major) frequencies ω and β as well as the (minor) harmonic frequencies $n(\omega - \beta) \pm \beta$, for positive integers n.

There are many unanswered questions that remain. First, this report has failed to cast this problem as one in bifurcation theory. If such a characterization is achieved in the future, one may expect a more fundamental understanding of the mechanics of the nonlinear solution as well as the fringe benefits that accompany all advanced, well-developed theories.

It would also be nice to know, for a given set of parameters, the exact frequency values at which the response switches between circles and annuli. Based on similar results for the van der Pol oscillator, these transition points should exist as analytic expressions thereby avoiding numerical iterations.

The asymmetric stiffness problem, which many reports have hypothesized as being the culprit of instability, is vastly more complex than the symmetric case. Preliminary Runge-Kutta solutions show not only that the circle/annulus plots become elliptic and occur with their axes rotated with respect to the y, z axes, but that there may be other shapes and more than one

transition point to consider. These problems, however, greatly extend the model's mimcry of an observed rotor's behavior.

This report is also limited to single forcing functions. Realistically, one must consider multiple forcing functions. Here again, superposition will fail for the nonlinear problem although it may be a first approximation. Certainly, harmonics (sums and differences of driving frequencies) may appear and could possible dominate. These problems appear to introduce no new theory, but do increase the computational complications.

Stability for all these problems remains the central focus. Even in the symmetric nonlinear problem with a single driver, it is still an open question of whether the response may move from an annulus to a circle (or vice versa) when it is perturbed.

7. References:

1. Childs, D. W., "The Space Shuttle Main Engine High-Pressure Fuel Turbopump Rotordynamics Instability Problem", Trans. ASME, Journal of Engineering for Power, Jan. 1978, pp. 48-57.

2. Childs, D. W., "Rotordynamic Characteristics of the HPOTP (High Pressure Oxygen Turbopump) of the SSME (Space Shuttle Main Engine)", NASA MSFC Contract NAS8-34505, Turbomachinery Laboratories Report RD-1-84, 30 January 1984.

3. Control Dynamics Company, "Effects of Bearing Deadbands on Bearing Loads and Rotor Instability", NASA MSFC Contract NAS8-35050, 20 January 1984.

4. Gupta, P. K., Winn, L. W., and Wilcock, D. F., "Vibrational Characteristics of Ball Bearings", Journal of Lubrication Technology, ASME Trans., Vol. 99F, No. 2, 1977, pp. 284-289.

5. Jeffcott, H. H., "The Lateral Vibration of Loaded Shafts in the Neighborhood of a Whirling Speed - The Effect of Want of Balance", Philosophical Magazine, Series 6, Vol. 37, 1919, p. 304.

6. Nayfeh, A. H., Perturbation Methods, J. Wiley & Sons, 1973.

7. Yamamoto, T. T., "On Critical Speeds of a Shaft", Memories of the Faculty of Engineering, Nagoya (Japan) University, Vol. 6, No. 2, 1954.

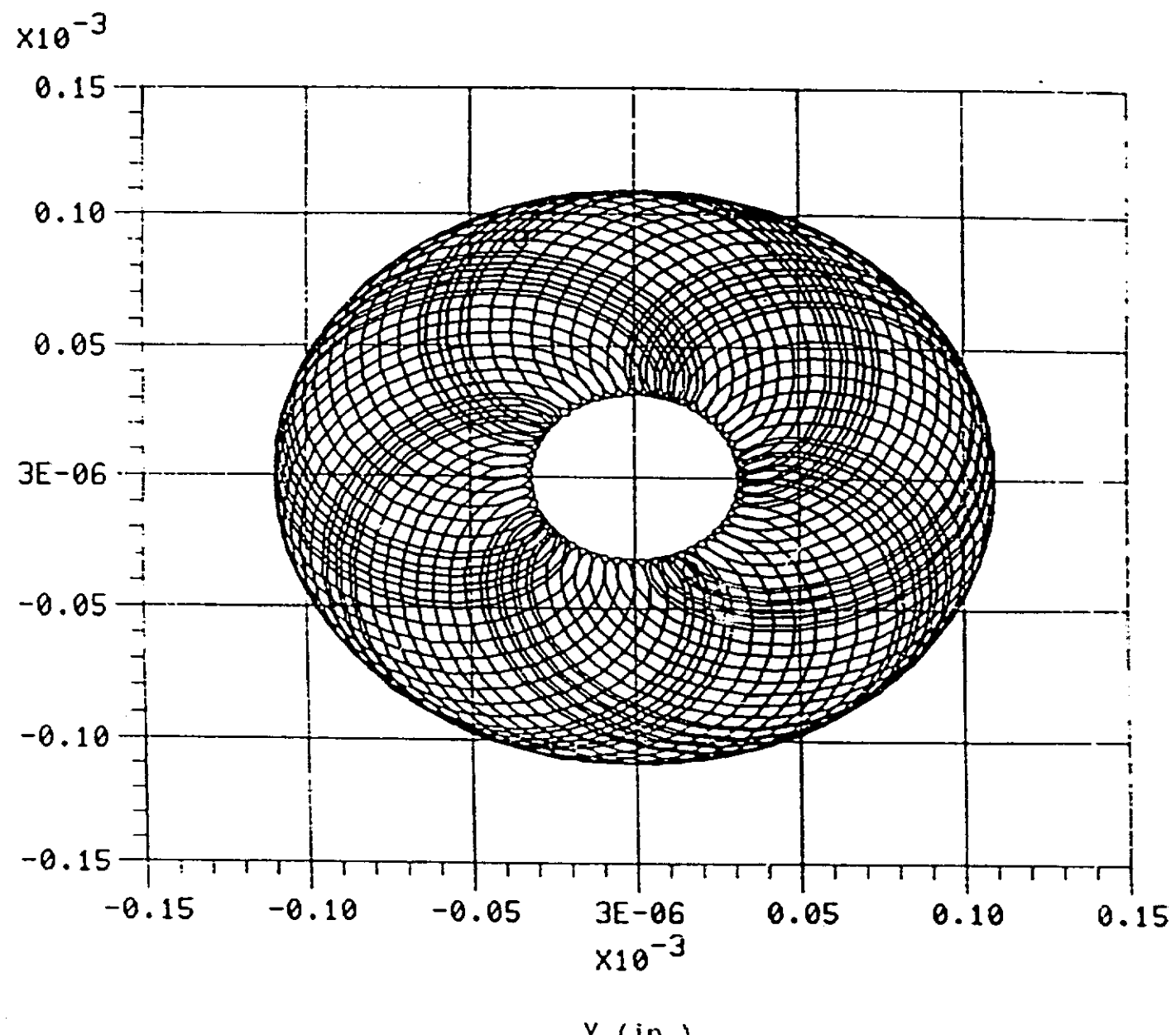

Figure 1

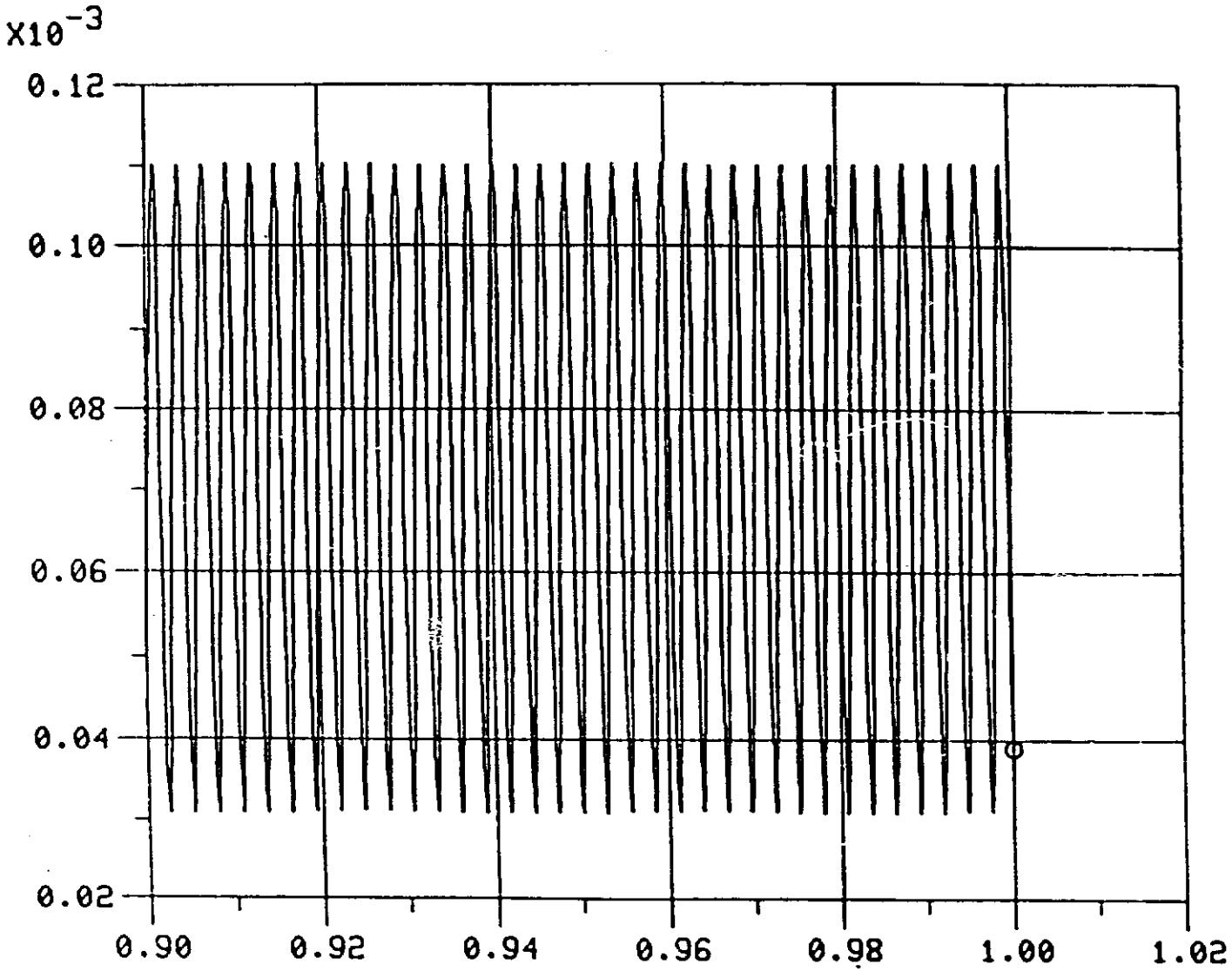

Figure 2

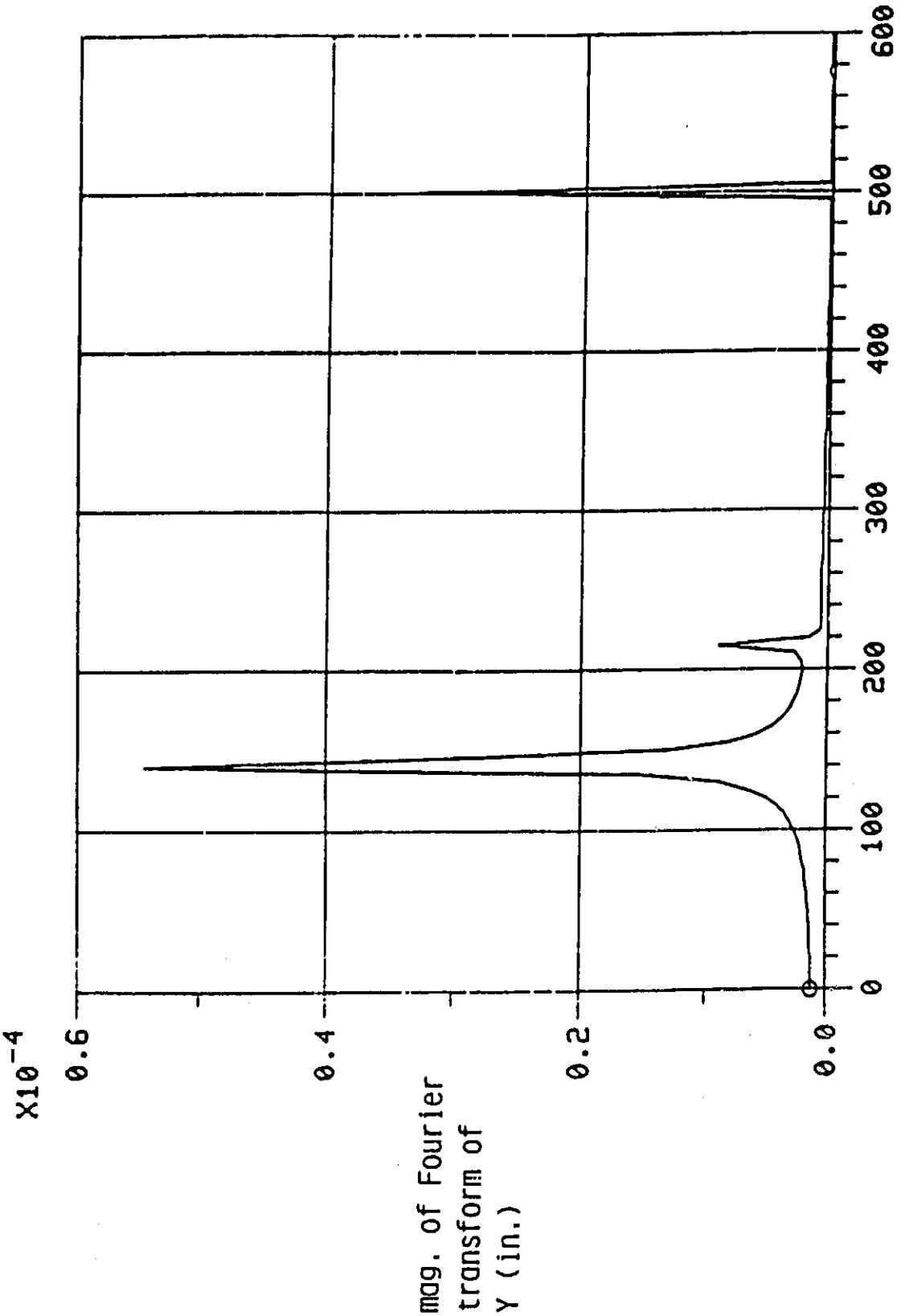

Figure 3

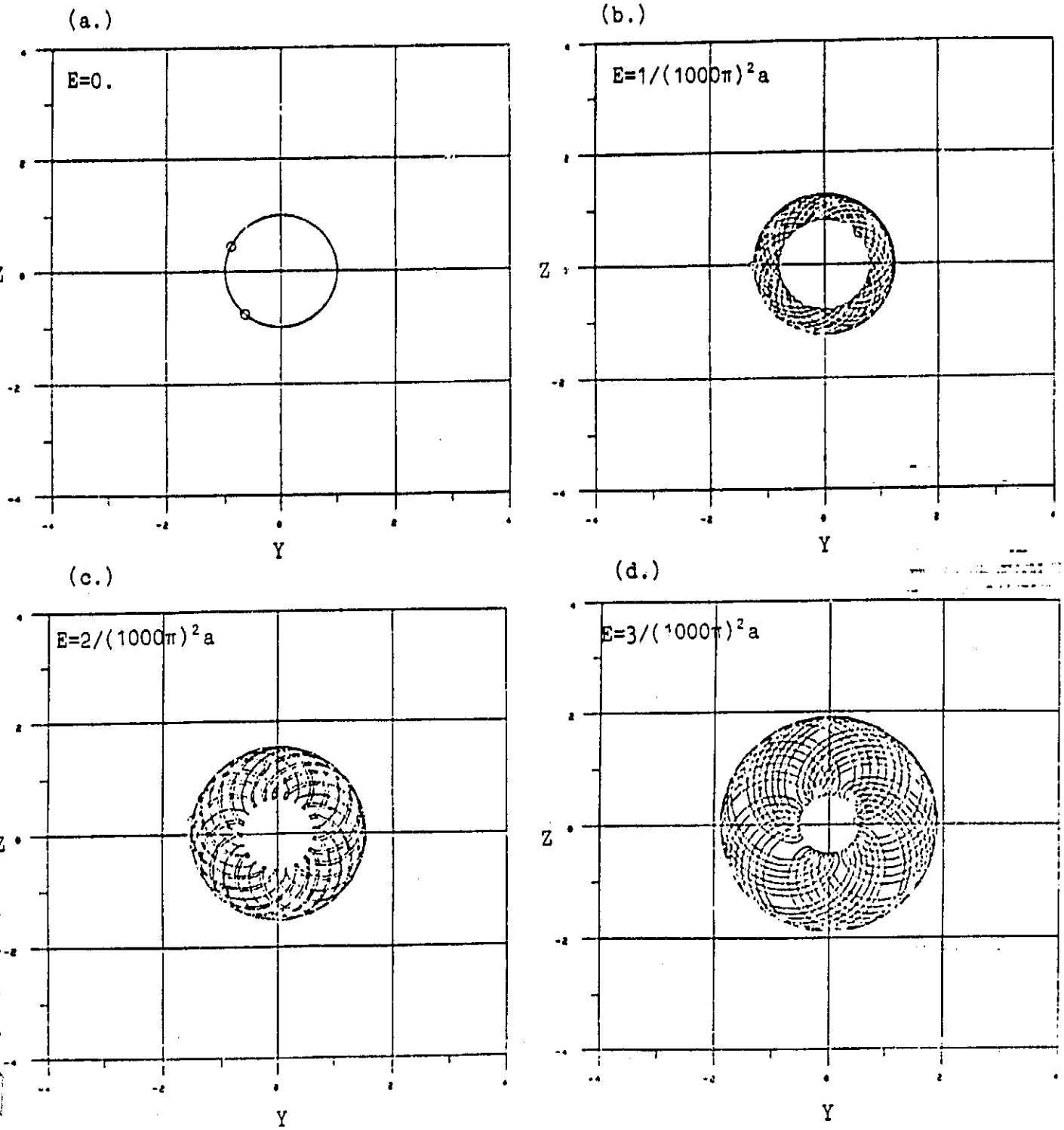

Figure 4

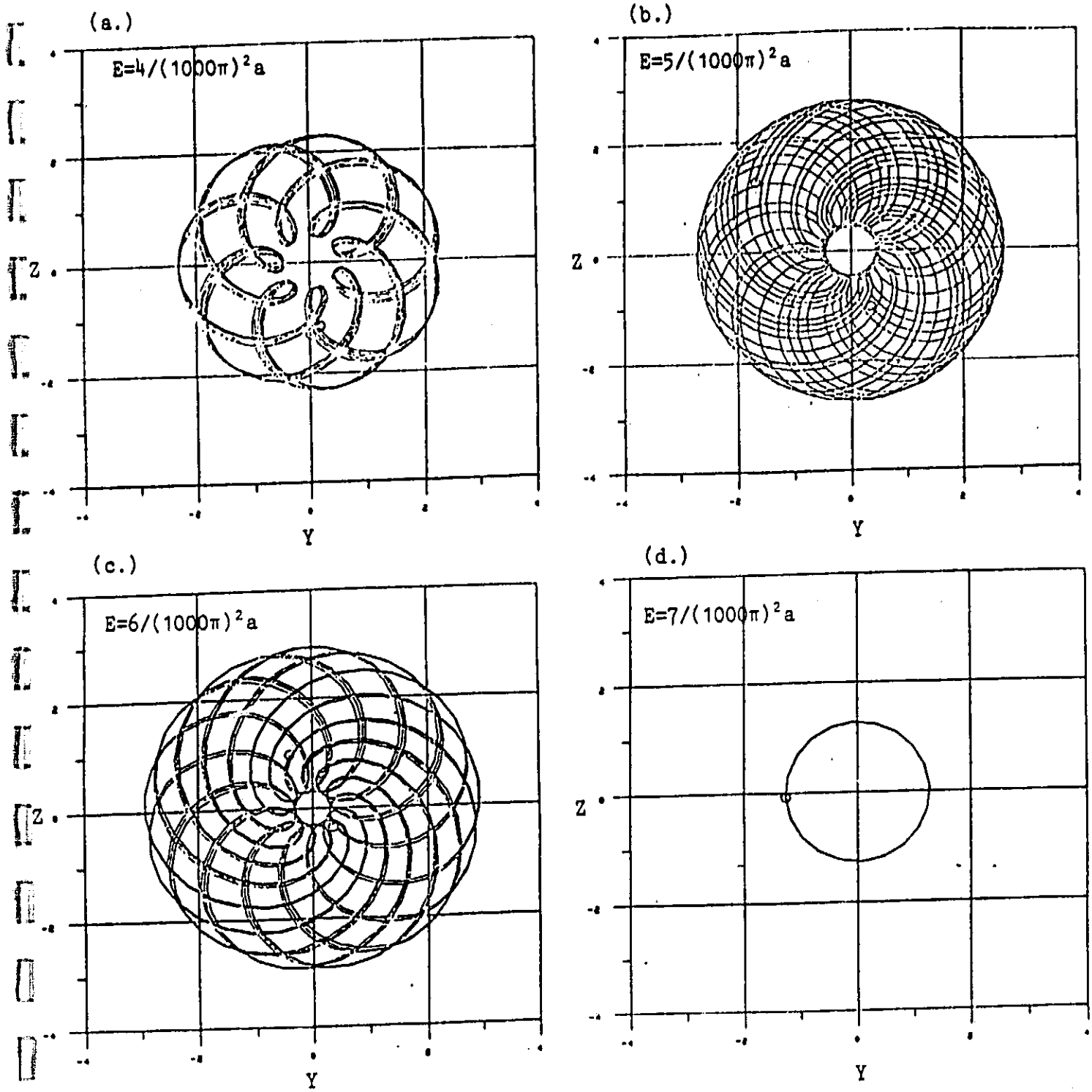

Figure 5

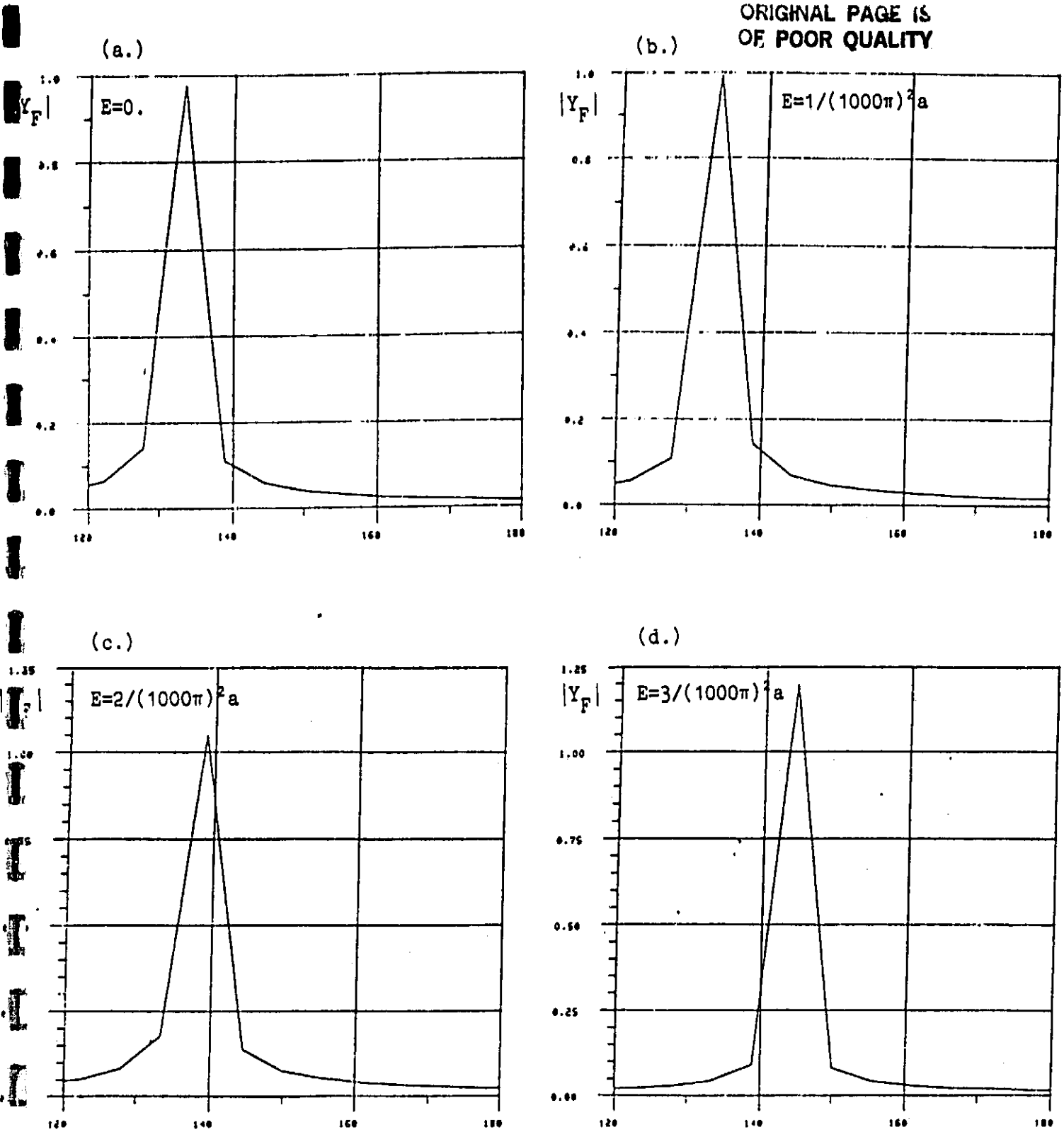

Figure 6

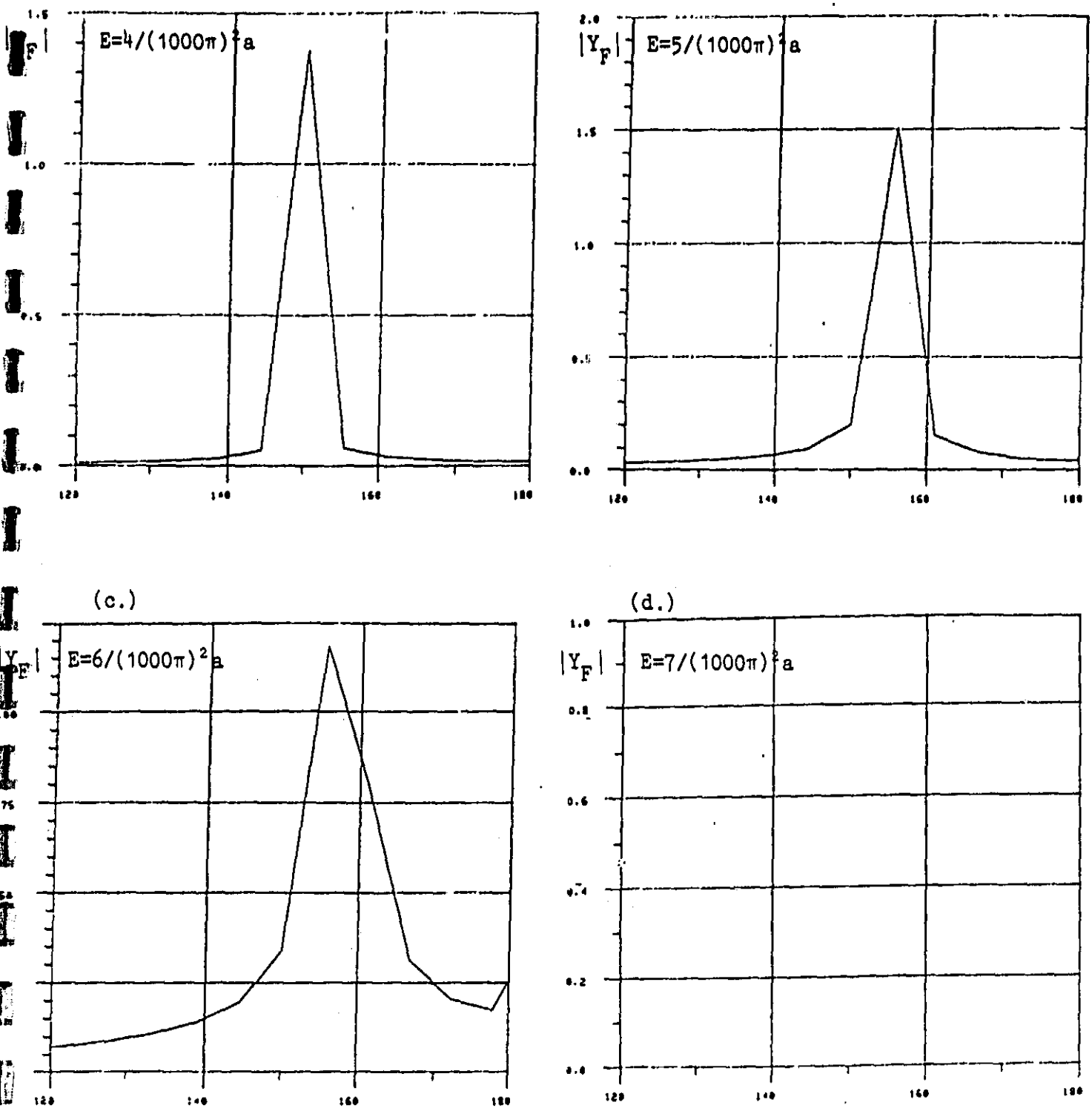

Figure 7

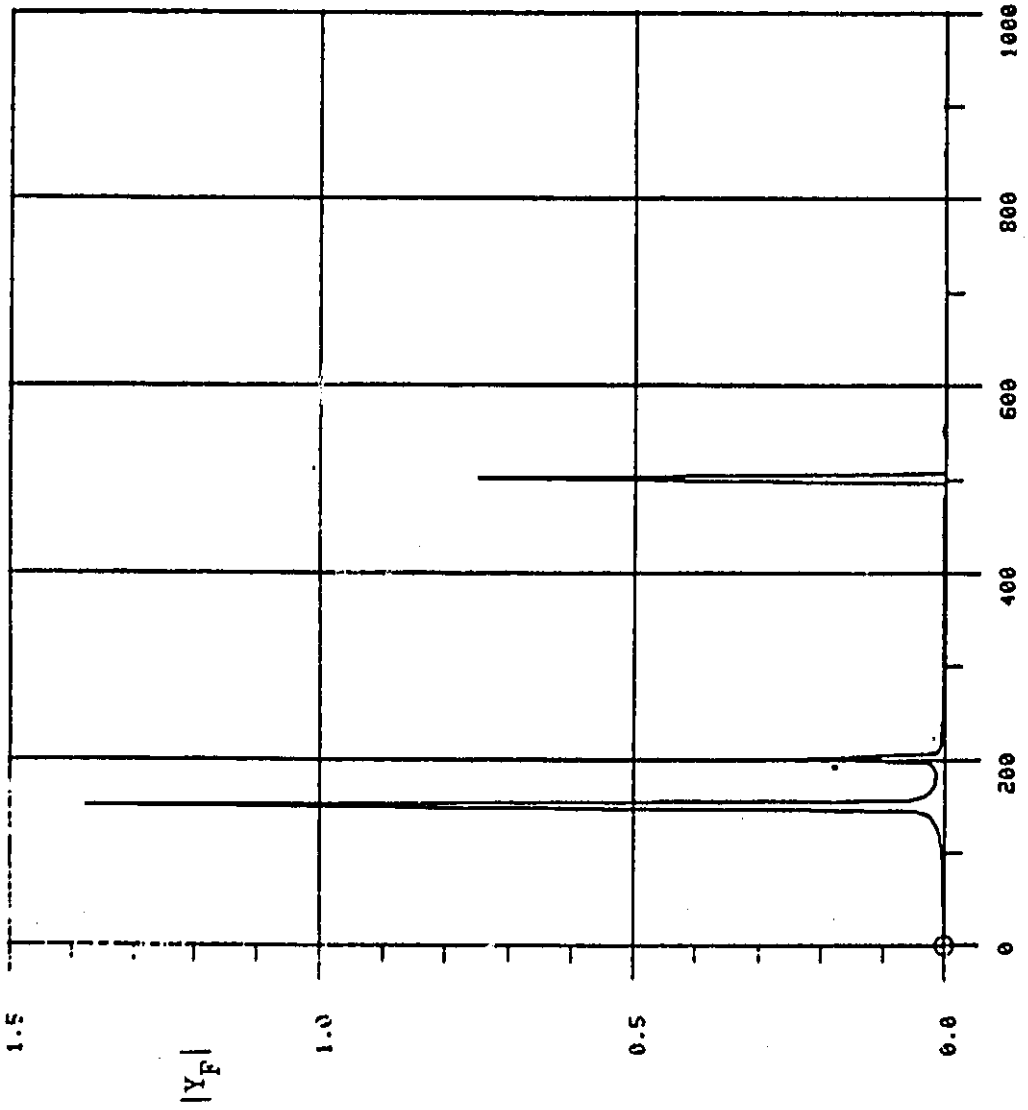

Figure 8

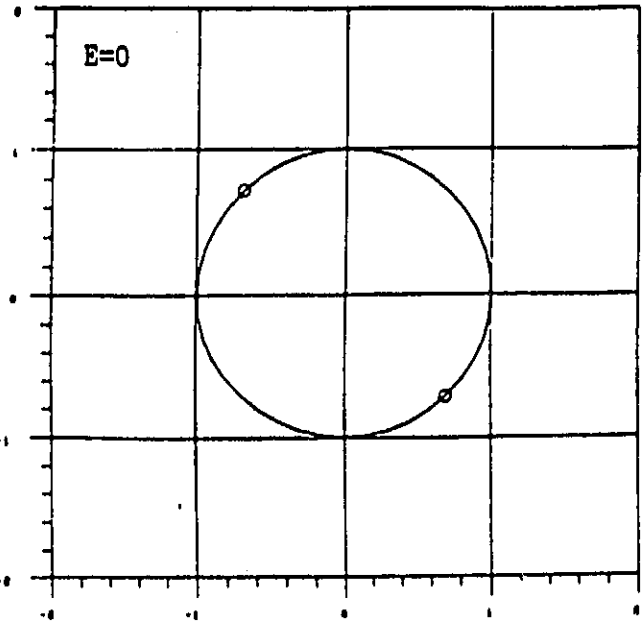

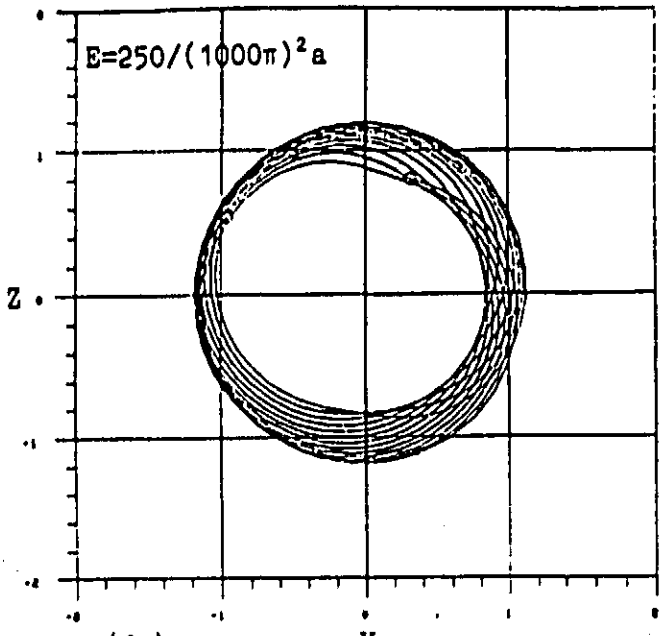

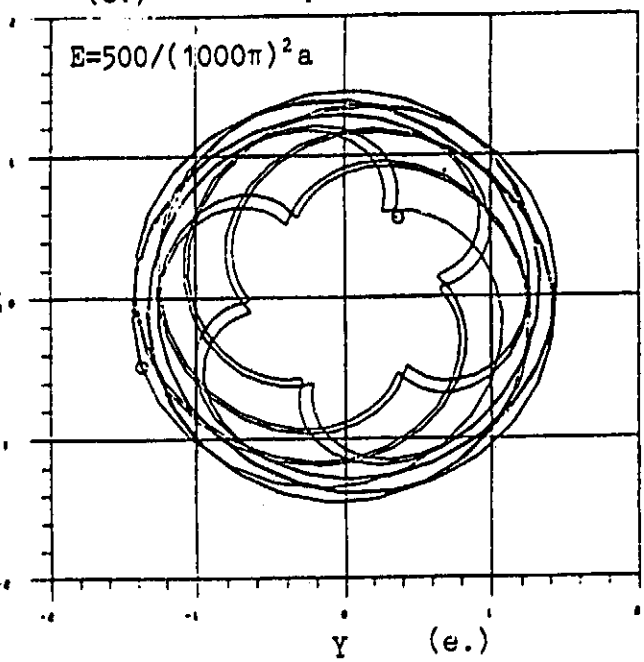

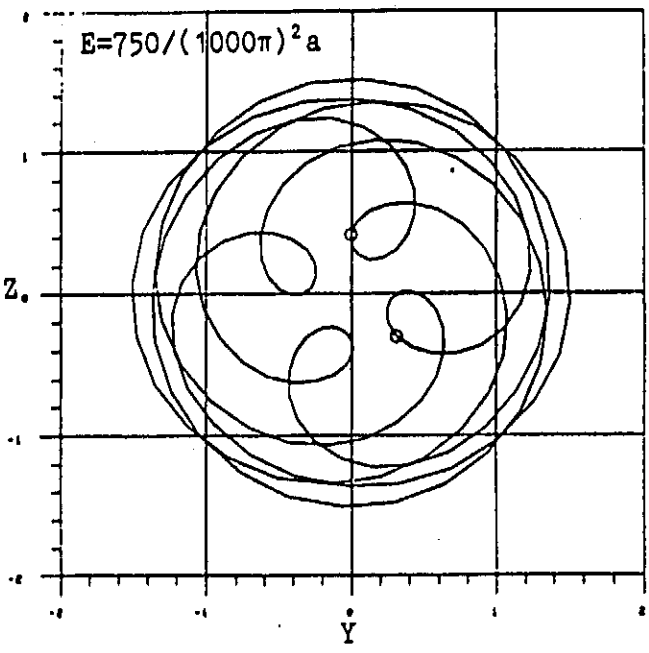

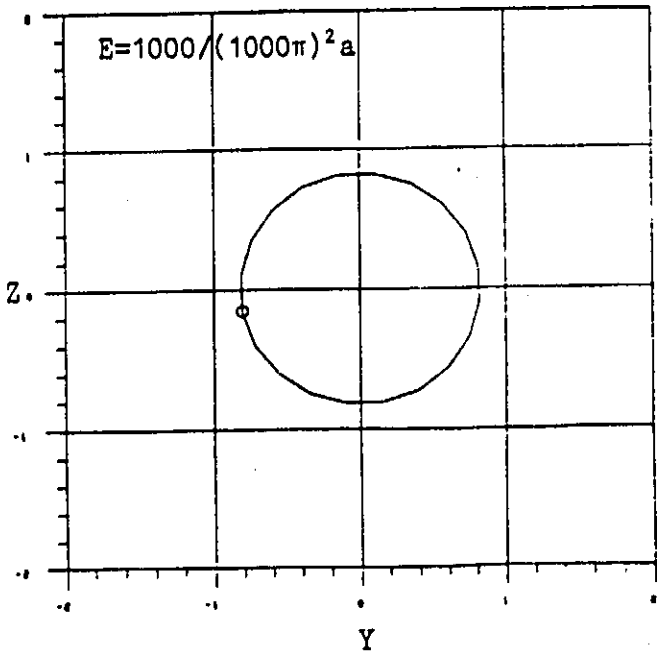

Figure 9

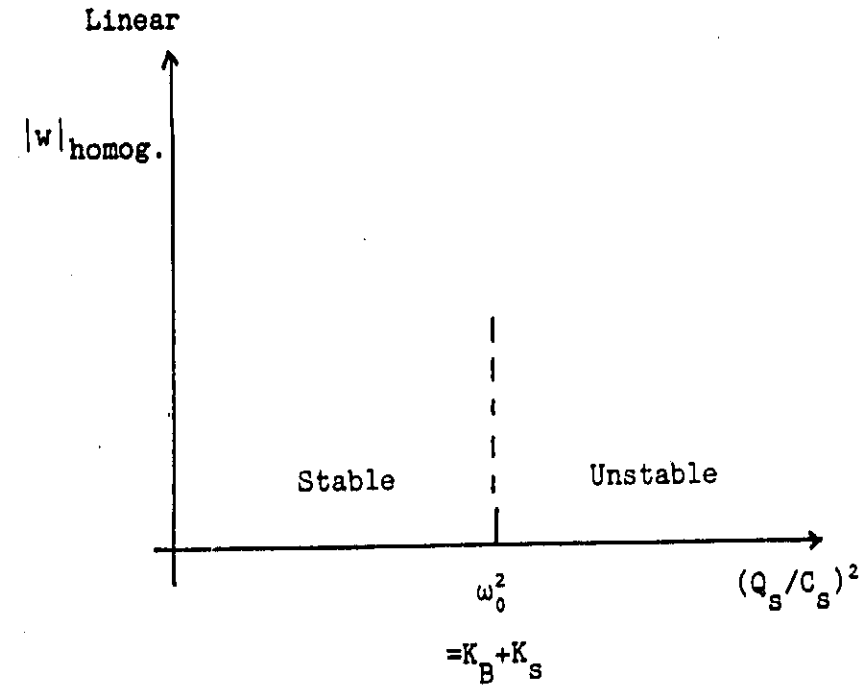

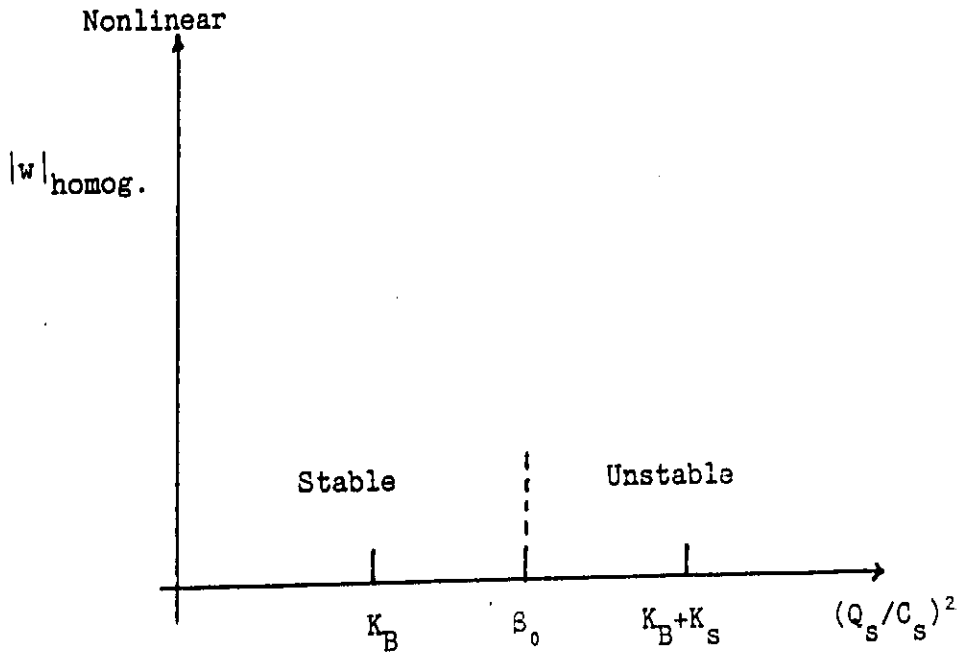

Figure 10

TABLE I
E = 0.5

ϕ	Shape (Circle/Annulus)	Radius (radii)	γ (Hz.)
0.0	C	2.137	-
0.1	A	2.130 - 2.145	115
0.2	A	2.105 - 2.169	97
0.4	A	1.959 - 2.305	61
0.5	A	1.747 - 2.470	41
0.53	A	1.618 - 2.549	34
0.54	C	1.597	-
0.6	C	1.833	-
0.7	C	2.441	-
0.8	C	3.656	-
0.9	C	6.954	-
0.92	C	8.249	-
0.93	A	1.212 - 4.018	13
1.0	A	1.369 - 3.230	40
1.2	A	1.551 - 2.858	81
1.4	A	1.643 - 2.822	118
1.6	A	1.648 - 2.748	154
1.8	A	1.694 - 2.633	190
2.0	A	1.804 - 2.679	222
2.2	A	1.939 - 2.830	263
2.4	A	1.993 - 3.162	294
2.6	A	1.632 - 3.125	333
2.8	A	1.533 - 2.864	370
3.0	A	1.528 - 2.769	410

TABLE II
E = 1.0

ϕ	Shape (Circle/Annulus)	Radius (radii)	γ (Hz.)
0.0	C	2.137	-
0.2	A	2.073 - 2.201	98
0.4	A	1.767 - 2.463	60
0.41	A	1.737 - 2.486	58
0.42	C	1.398	-
0.5	C	1.650	-
0.6	C	2.118	-
0.8	C	4.548	-
0.9	C	9.174	-
0.97	C	18.524	-
0.99	C	10.436	-
1.0	A	.872 - 2.033	12
1.2	A	1.003 - 4.194	68
1.4	A	1.145 - 3.972	96
1.6	A	1.431 - 3.839	145
1.8	A	1.151 - 3.283	185
2.0	A	1.341 - 3.296	222
2.2	A	1.598 - 3.499	256
2.4	A	1.871 - 3.932	286
2.6	A	1.732 - 4.456	322
2.8	A	1.062 - 3.745	357
3.0	A	.981 - 3.390	400

TABLE III
E = 1.5

ϕ	Shape (Circle/Annulus)	Radius (radii)	γ (Hz.)
0.0	C	2.137	-
0.2	A	2.040 - 2.230	96
0.3	A	1.885 - 2.371	78
0.35	A	1.755 - 2.476	68
0.36	C	1.364	-
0.4	C	1.449	-
0.6	C	2.398	-
0.8	C	5.427	-
0.9	C	11.269	-
0.98	C	27.247	-
0.99	C	25.102	-
1.0	C	19.448	-
1.2	C	2.585	-
1.38	C	2.028	-
1.39	A	.357 - 4.628	99
1.4	A	.529 - 4.832	100
1.6	A	.837 - 4.660	139
1.77	A	.359 - 3.832	172
1.78	C	1.717	-
1.8	C	1.709	-
1.91	C	1.676	-
1.92	A	.100 - 3.121	195
2.0	A	.496 - 3.282	217
2.2	A	1.062 - 4.076	250
2.4	A	1.496 - 4.564	286
2.6	A	1.692 - 5.341	312
2.8	A	.222 - 3.987	359
2.81	C	1.565	-
2.9	C	1.560	-
3.0	C	1.555	-